Gamma Cross Sections

Daniel Babnigg

October 31 2024

1 Introduction

Counting particle experiments are used to determine which models in the fields of high energy particle and nuclear physics are plausible, and which models do not make sense given experimental data. In this experiment, three different gamma-emitting (radioactive) sources are used to measure the total interaction cross section for gammas around 30 keV to 1.25 MeV, specifically for aluminum (Al). The radioactive elements are Na-22, Ba-133, and Cs-137. Different linear attenuation coefficients are then calculated, then compared to a predicated model.

A NaI+PMT gamma detector is used, where raw counts are shown in the USX software, a pulse-height analyzer. A PMT high voltage is supplied from the PHA, where +900 V was used. Coarse and fine gain settings adjusted so the important features of a given spectra can be well-recorded in the channels. Known energies are well-known for the gammas of radioactive source, which made it possible to guarantee that the full features were present on the spectrum.

2 Results

The USX pulse-height analyzer software had built-in tools that were convenient for calibrating and measuring a spectrum. Using ratios, one could verify that the features shown on the channels did indeed correspond to theoretical energies. There were 2 point and 3 point calibrations available, which calibrated 2 or 3 channels to energies using a 1st or 2nd degree polynomial, and this simple calibration allowed for each channel to match to an energy.

There was also a region of interest (ROI) feature, where an area of the spectrum could be highlighted, and the program will fit a background, a Gaussian, and return statistics. Most importantly, it gave gross counts, net counts, and a centroid. The centroid calculation allowed for more accurate calibration, and the gross and net counts were used to help calculate the linear attenuation coefficients.

2.1 Spectrum Identification and Fitting

Three radioactive sources were used in this experiment: Cs-137, Na-22, and Ba-133. It is important to first properly identify features on each spectrum before attempting to take measurements. After identifying features, each full energy peak was modeled, where a Gaussian with background was fit to the channel data. For this section, there was no aluminum used since the purpose of this analysis is to first understand each of the sources independently.

Each spectrum can show full energy peaks, which happens when a photon deposits its energy in the detector, and a Gaussian will be centered on the true photon energy by the central limit theorem. There can also be a Compton shelf, which is where a photon may Compton scatter before escaping from the detector, meaning only some of the full energy will be deposited in the detector, creating a plateau. The maximum energy transfer occurs when a photon is scattered through an angle of 180°, and this limit is called the Compton edge. Finally, some photons may initially travel away from the detector but scatter back into the detector, which are called backscatter photons. It is most likely to see 180° backscatters, which creates a backscatter peak.

Cs-137 has two gammas - one at 32.2 keV, and one at 662 keV. In Figure 1, both of these peaks are clear and labeled, and can be identified because of their Gaussian-like shape. Also annotated is the Compton shelf, which is a raised area above the noise level, and it ends at the labeled Compton edge. There is an additional peak that is not an energy peak, so it is likely the backscatter peak.

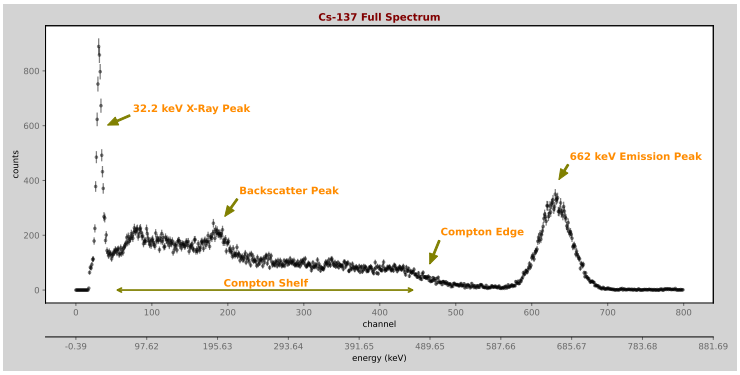

Figure 1: Cs-137 full annotated spectrum.

Na-22 also has two gammas, one at 511 keV and the other at 1.2746 Mev. These two peaks are Gaussian-like, and are annotated in Figure 2. Unlike Cs-137, the lower energy peak has significant detection area to its left - therefore, both a Compton shelf and a Compton edge can be seen for both peaks, which are all annotated on the plot. There is one other peak in the graph, and since it is not Gaussian-like, it is most likely the backscatter peak. It is fair to assume that this is a shared backscatter peak.

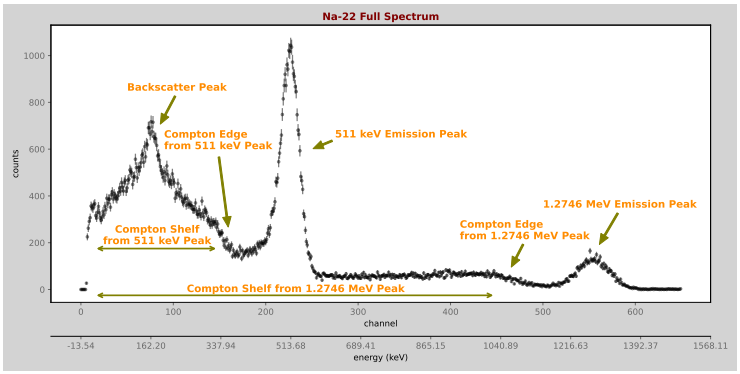

Figure 2: Na-22 full annotated spectrum.

Ba-133 has three clear gammas: one at 31 keV, one at 81 keV, and one at 356 keV. However, there are also other less significant gammas at 276 keV, 302 keV, and 382 keV that contribute. The first two energies are clear and gaussian-like, shown in Figure 3. The 356 keV emission peak is also near gaussian, but is mixed with the other energies. Because the 356 keV emission is more common than the energies near it, it dominates the shape, but the other peaks still contribute a visible amount. The approximation of where each of these four higher energies are also annotated in Figure 3. These four peaks are also referred to as the mixed peaks, where all contribute to what appears to be a Compton shelf and Compton edge. Finally, between the 31 and 81 keV peaks, there is another non-gaussian peak - it can be assumed that this is the backscatter peak, with potential contribution from a Compton edge for the 81 keV peak.

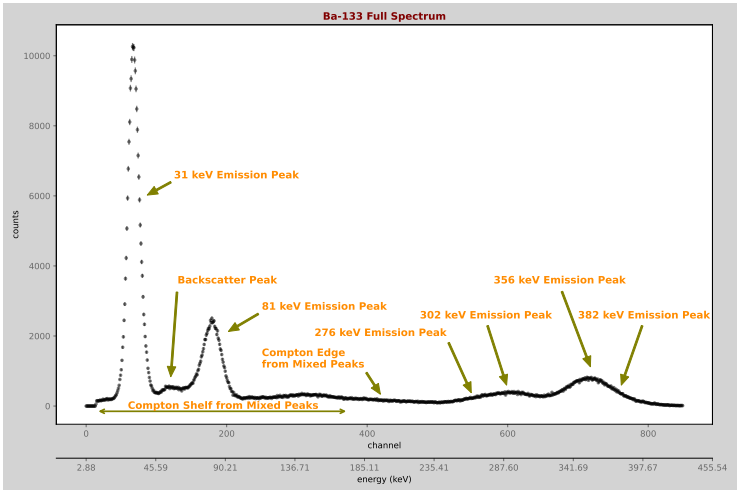

Figure 3: Ba-133 full annotated spectrum.

Now that the features of the spectra are identified, the full peaks can be fit. A specific area is chosen for the fit, to try to get as much background as possible on either side of the peak - the fitted area corresponds to the range of the graph. Note that for each count, there is an uncertainty which is simply the square root of the counts ($\sqrt{N}$). Plotted on each Gaussian fit figure is the original data, the best-fit functional forms, the parameters with uncertainties, and the goodness-of-fit parameters. A fitter is used on python, which accounts for those uncertainties, and fits a Gaussian with a linear background term to the data over a given range of channel:

$$\mathbf{f}(\mathbf{x}) = \frac{\mathbf{N}}{\sqrt{2\pi}} e^{-\frac{(x-\mu)^2}{2\sigma^2}} + \mathbf{m}x + \mathbf{b} \tag{1}$$

The fitted parameters in Equation 1 are bolded: N, μ, σ, m, and b. Note that the fit is done using the channels as x, but the calibrated energies are also shown on the figures. Additionally, the fit is able to produce best-of-fit parameters, like χ^2, N, and χ^2/N. N is the degrees of freedom, not to be confused with N from the fit. In each figure, a Gaussian without the background term is also fit, and its reduced χ^2 is annotated along with its best-fit function for comparison in purple. A reduced χ^2 of approximately 1 will be considered as good in the following examples.

Gaussian fits, with and without background, were performed on both the Cs-137 peaks at 32.2 keV and 662 keV. The fit to the 32.2 keV peak, shown in Figure 4, makes it clear both qualitatively and quantitatively that the background term is important in the fit, with the reduced χ^2 being significantly lower when a background term is added. However, even with the background term, the reduced χ^2 is not good, being significantly over 1 - the peak looks asymmetric, the background may be more complex than linear, and there are not as many data points when compared to other fits - all of these can contribute to the inaccurate fit. The 662 keV peak fit, shown in Figure 5, provides a much more accurate fit. The reduced χ^2 is around 1, and the Gaussian is qualitatively very close to the data, given the uncertainties. Like the 32.2 keV peak, the background term improves the fit, and the background for this peak follows the data well.

Fits were also performed for the two Na-22 full energy peaks at 511 keV and 1.2746 MeV energies. The fit to the 511 keV peak is shown in Figure 6, and the background is clearly very significant for this example, with the reduced χ^2 significantly decreasing when a background term is added. The reduced χ^2 with background is not around 1, and the fit is not great - it seems that the background is not truly linear, as it seems to have a positive derivative on the left side of peak, and a negative derivative on the right side of the peak. Additionally, the peak appears to be slightly asymmetric, and both of these factors likely contribute to why the peak is not fit perfectly. The fit for the 1.2746 MeV peak is shown in Figure 7. Consistent with all the other peaks, the background term is important and produces a better fit with a smaller reduced χ^2. The reduced χ^2 is around 1, and this fit is accurate to the data. It perhaps

is not as good as some of the other fits, which can be due to low counts and therefore relatively high uncertainties on the data.

Gaussians were also fit for the first two energies of Ba-133, at 31 keV and 81 keV. The fit to the 31 keV peak, shown in Figure 8, shows very high signal in the counts; however, the fit even with the background term is not great, since its reduced χ^2 is not close to 1. The background appears to be approximately linear, but the actual peak seems to be both asymmetric and slightly flat-top, which means something non-Gaussian may better describe this peak. For the fit to 81 keV, shown in Figure 9, the Gaussian much better describes the peak. The background is significant in this example, with a large reduction in the reduced χ^2, and the reduced χ^2 with background is close to 1. This is a good fit, and qualitatively the background and the Gaussian peak follow the data well.

A single Gaussian was attempted to be fit for the 356 keV peak in Ba-133, but it failed due to the aforementioned complexity in this peak - there are also peaks at 276, 302, and 382 keV that mix and interact with the strong 356 keV peak. As shown in Figure 10, the single peak describes the data poorly. However, by adding 4 Gaussians for each peak with a shared linear background, the fit improves significantly, with a reduced χ^2 of around 1. Qualitatively, the mixed Gaussian also follows the data extremely well. The single Gaussians for each energy are also plotted, and are qualitatively close to the physical expectations - the centers of the peaks are separated and are close to the expectations and the strongest peak is at 356 keV. Even though the parameters were free and the four Gaussians could optimize with any centers and ampltiudes, they still are consistent with the physical expectation.

In summary, the reduced χ^2 values imply that the 662 keV peak for Cs-137, the 1.2746 MeV peak for Na-22, and the 81 keV peak for Ba-133 were the best fits. The 356 keV peak was only fit well when a multi-Gaussian component was used. The other peaks were not fit well due to various factors, such as asymmetry in the Gaussian peak, low signal to noise, and a non-linear background.

2.2 Extracting linear attenuation coefficients

With a better understanding of the full energy peaks for Cs-137, Na-22, and Ba-133, now linear attenuation coefficients could be calculated. In order to calculate linear attenuation coefficients for each peak, the thickness of the Aluminum used must be plotted against a normalized count rate. Then, the linear attenuation coefficient is λ in Equation 2:

$$R/R_0 = e^{-\lambda x} \tag{2}$$

The count rate is $R = N/t$, and was normalized by dividing R by R_0, the count rate when there was 0 Aluminum thickness. N is the net counts in the peak, calculated using the ROI feature on the USX software, where it returns both gross and net counts of a fitted region. The net counts were background subtracted, where the background was simply calculated using a linear line from the noise level on the left and right side of the fitting region. There was therefore

high variation on the net counts depending on the region of interest bounds that was selected, and therefore high care was put into deciding where this region of interest was to make sure the left and right bounds captured background, while not including too much non-peak noise.

The uncertainty on R/R_0 impacted the uncertainty on the linear attenuation coefficient, and needed to be accurately calculated. The uncertainty in R/R_0 depends on N and t, for both a given thickness and thickness 0. Since N = gross - background counts, the uncertainty on the net counts was calculated using Equation 3:

$$\Delta(net) = \sqrt{(\Delta gross)^2 + (\Delta background)^2} = \sqrt{(\Delta gross)^2 + (\Delta(gross - net))^2} \tag{3}$$

where $(\Delta gross) = \sqrt{gross}$ and $(\Delta(gross - net)) = \sqrt{gross - net}$. therefore,

$$\Delta(net) = \sqrt{2 * gross - net} \tag{4}$$

(Δt) was always 0.5 since the time read out in integers, and uncertainty on R was calculated using Equation 5:

$$\frac{\Delta R}{R} = \sqrt{\left(\frac{\Delta net}{net}\right)^2 + \left(\frac{\Delta t}{t}\right)^2} \tag{5}$$

Equation 5 was used to calculate R and R_0, leading to the final uncertainty on R/R_0, the ratio, in equation 6:

$$\frac{\Delta R/R_0}{R/R_0} = \sqrt{\left(\frac{\Delta R}{R}\right)^2 + \left(\frac{\Delta R_0}{R_0}\right)^2} \tag{6}$$

Plots are provided with all rates vs thickness for the Cs-137 32.2 keV and 662 keV peaks, the Na-22 511 keV and 1.2746 MeV peaks, and the Ba-133 31, 81, and 356 keV peaks. An iterative process was used to calculate the rates and the uncertainty on the rates, and the input was the gross and net counts, along with the time. R/R_0 and its uncertainty only depends on these quantities. The rates were calculated for a range of Aluminum thickness, where the uncertainty in thickness was negligible. Data was taken until the R/R_0 went under .5, and the plot looked like exponential decay.

Based on the reduced χ^2 values, good fits were present for both Na-22 keV peaks in Figures 13 and 14. The fit for the 32.2 keV peak in Cs-137 was okay, shown in Figure 11. The fits were not good for the 662 keV peak in Cs-137 shown in Figure 12, and all peaks for Ba-133 at 31, 81, and 356 keV shown in Figures 15, 16, and 17.

3 Discussion and Conclusion

Synthesizing the results from the previous sections, there are now calculated linear attenuation coefficients for each energy, shown in Table 1. Additionally,

these results are plotted in Figure 18 where the calculated linear attenuation coefficients and uncertainties are plotted in black, NIST data are plotted in orange, and interpolated values at the same energies studied are shown in brown. The interpolation used a bicubic spline which describes the trend well, and the uncertainties on the NIST data are 3%. NIST gives the coefficients in units cm^2/g, so they are multiplied by the density of aluminum $\rho = 2.710 g/cm^3$. The final agreement with theoretical values is shown in Figure 19, where the y-axis is the theoretical minus experimental coefficients.

Energy (keV)	**Linear Attenuation Coefficient (cm^{-1})**
31.0	2.112 ± 0.011
32.2	1.72 ± 0.05
81.0	0.471 ± 0.006
356.0	0.304 ± 0.006
511.0	0.214 ± 0.002
662.0	0.212 ± 0.002
1274.6	0.148 ± 0.005

Table 1: Linear Attenuation Coefficients for analyzed Energies.

It seems that, in general, the best agreement comes with higher energies. These results are consistent, such as for the 662 keV peak, which had a good Gaussian fit and an okay linear attenuation fit. The 356 keV peak in Ba-133 is one with a significant residual, but that is easily explained by the fact that the Gaussian was interfered by the other peaks at the location. The worst residuals are at all low energies - 31.0, 32.2, and 81.0 keV. The residuals were all positive, meaning that the experiment under approximated the theoretical linear attenuation coefficient.

However, the errors in both the Gaussian fits to the peaks and the error in the attenuation coefficient seem to be dominated rather by a large error in low energies from some other systematic. The photoelectric effect becomes more and more prevalent at lower energies, which could have impacted the experiment.

The ROIs could have been selected to more accurately calculate the net counts, which impacts the attenuation coefficient. The background is approximated as a line, but the true background could have diverged from that - another more complex method of background calculation, like a quadratic, may have led to better results. Also, changing the gain settings to make the lower energy peaks more pronounced (more channels per peak) could have led to better data collection. In conclusion, there seems to be fair agreement with theoretical linear attenuation coefficients for high energies.

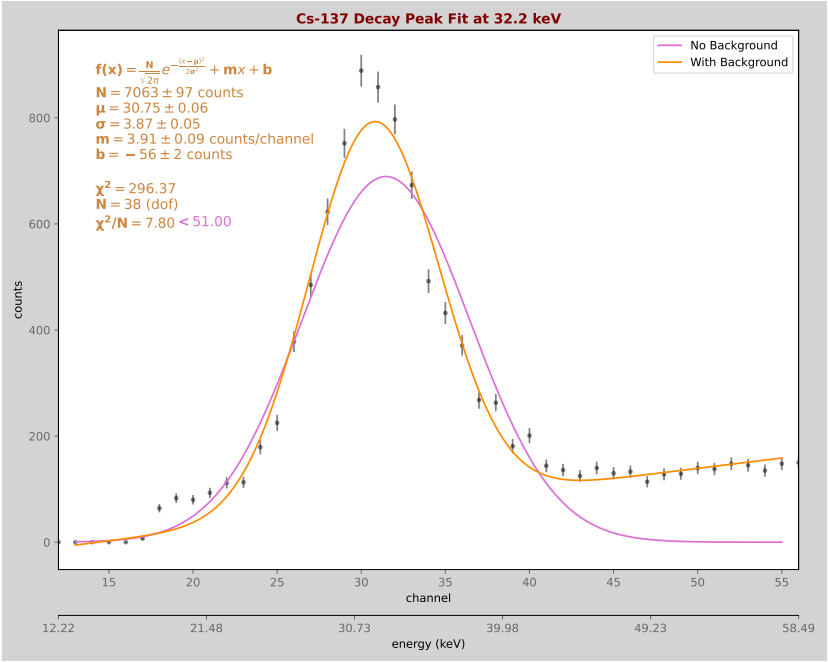

Figure 4: Gaussian with linear background fit for Cs-137 32.2 keV peak.

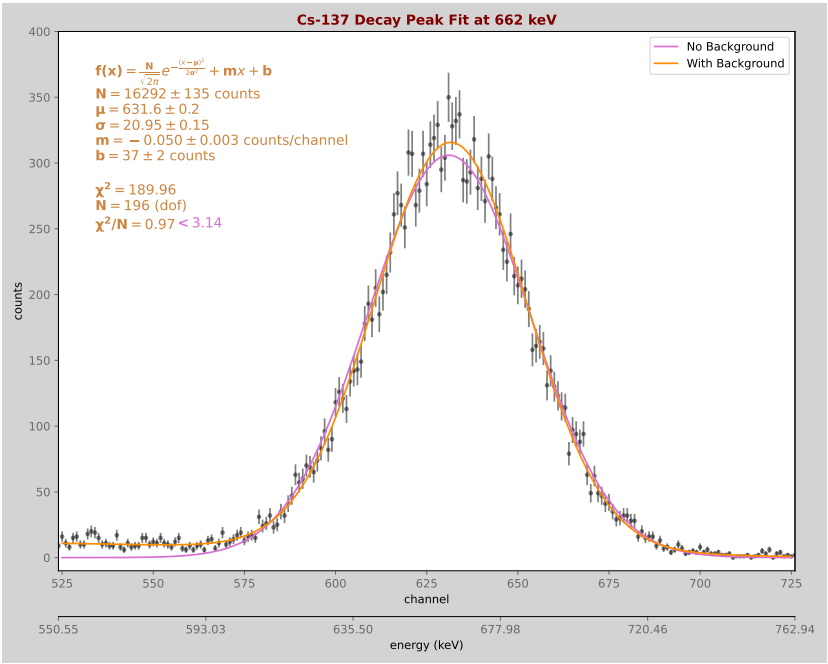

Figure 5: Gaussian with linear background fit for Cs-137 662 keV peak.

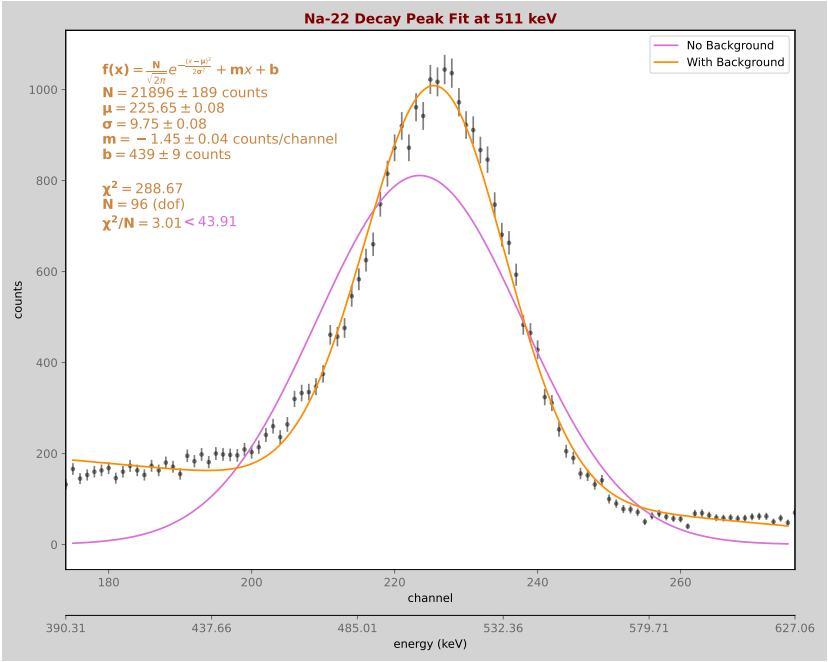

Figure 6: Gaussian with linear background fit for Na-22 511 keV peak.

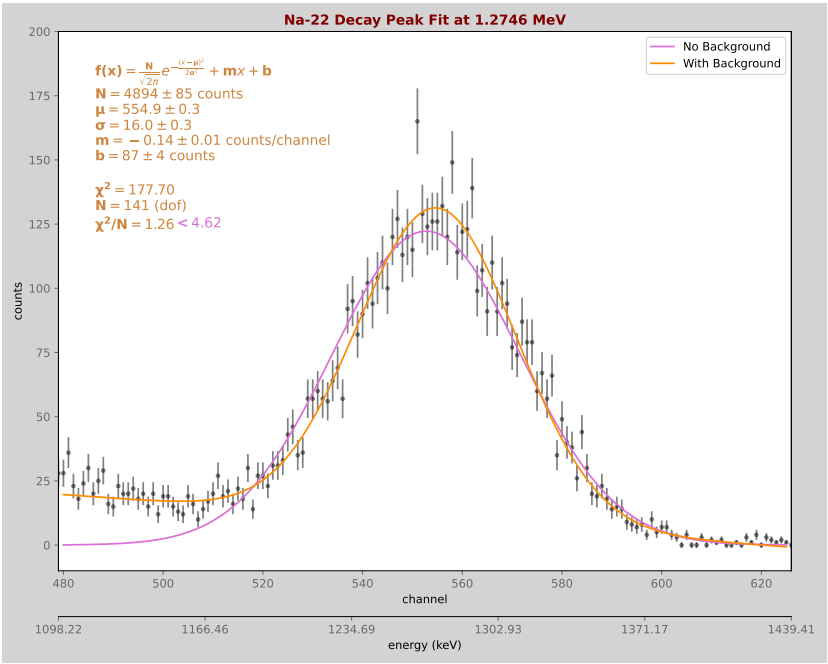

Figure 7: Gaussian with linear background fit for Na-22 1.2746 MeV peak.

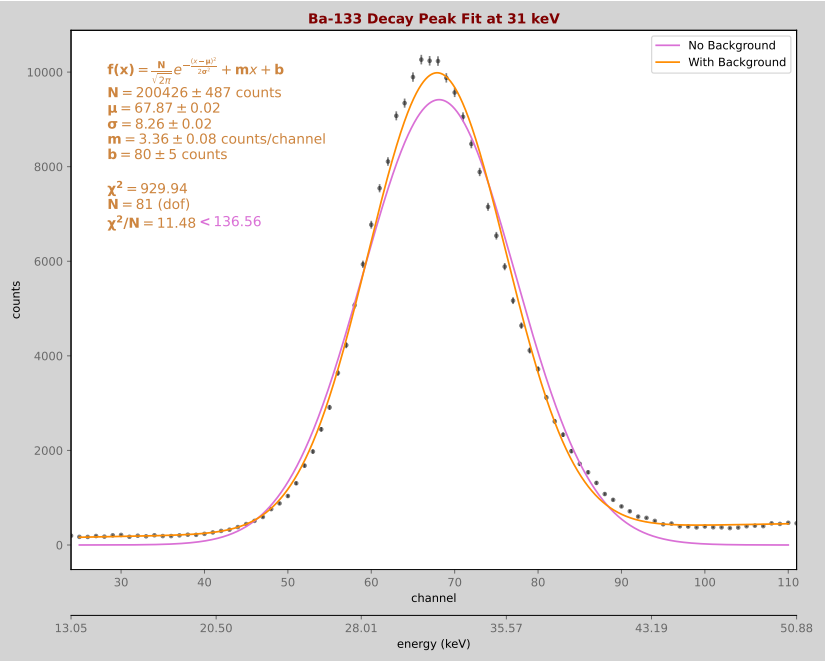

Figure 8: Gaussian with linear background fit for Ba-133 31 keV peak.

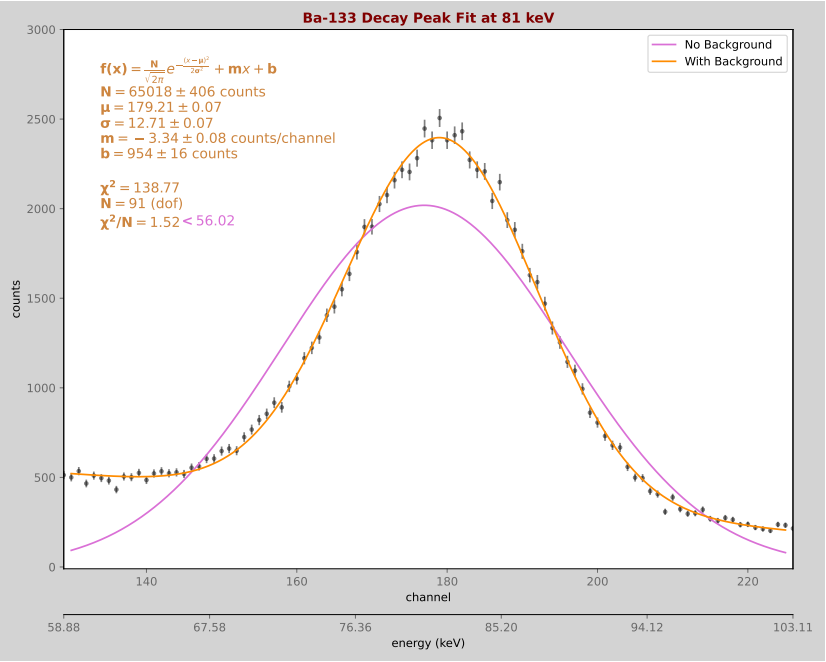

Figure 9: Gaussian with linear background fit for Ba-133 81 keV peak.

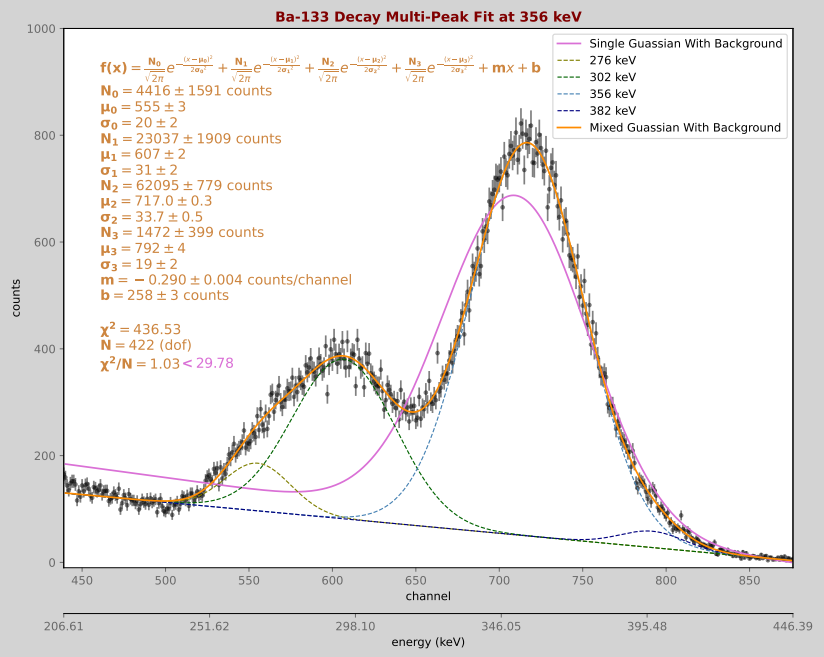

Figure 10: Multi-component gaussian with linear background fit for Ba-133 276, 302, 356, 382 keV peaks.

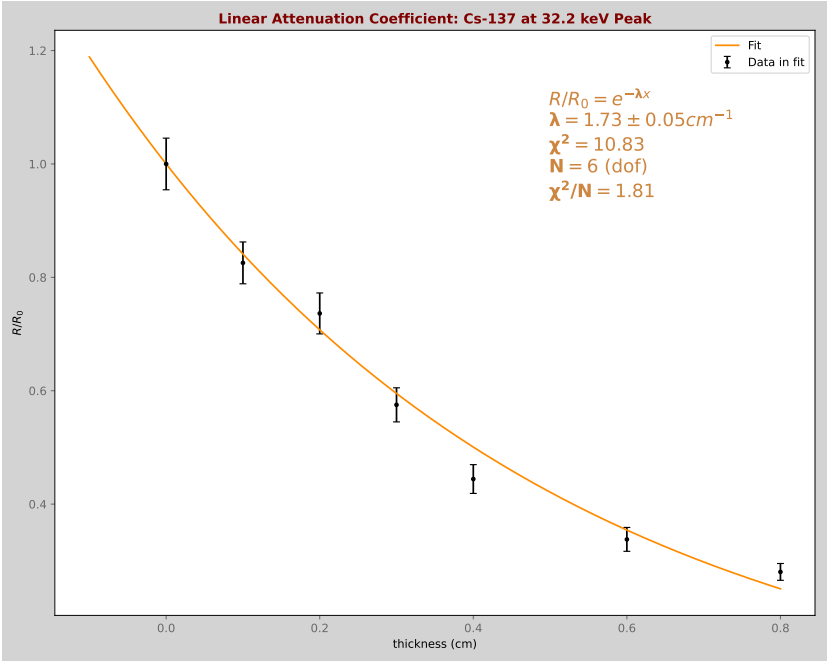

Figure 11: Linear attenuation coefficient fit for Cs-137 at 32.2 keV peak.

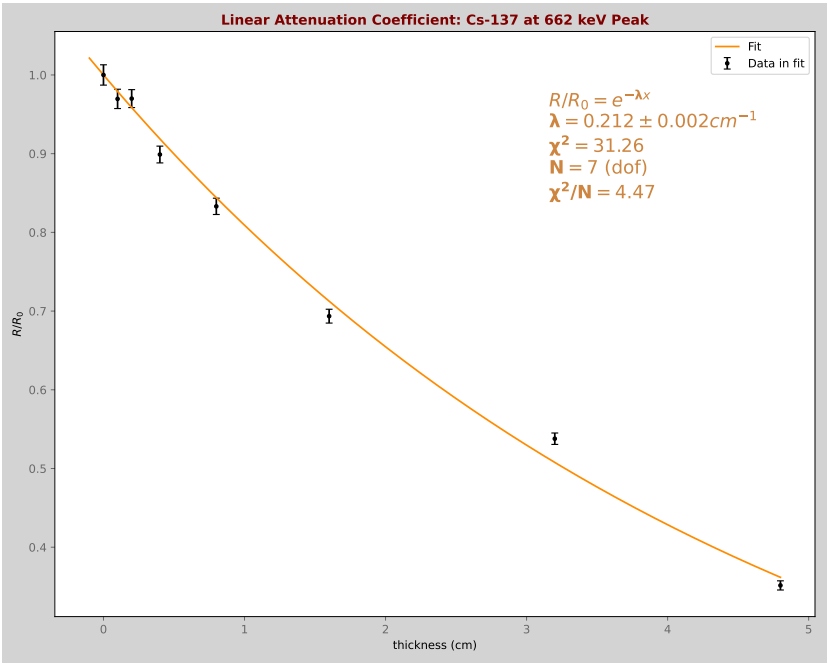

Figure 12: Linear attenuation coefficient fit for Cs-137 at 662 keV peak.

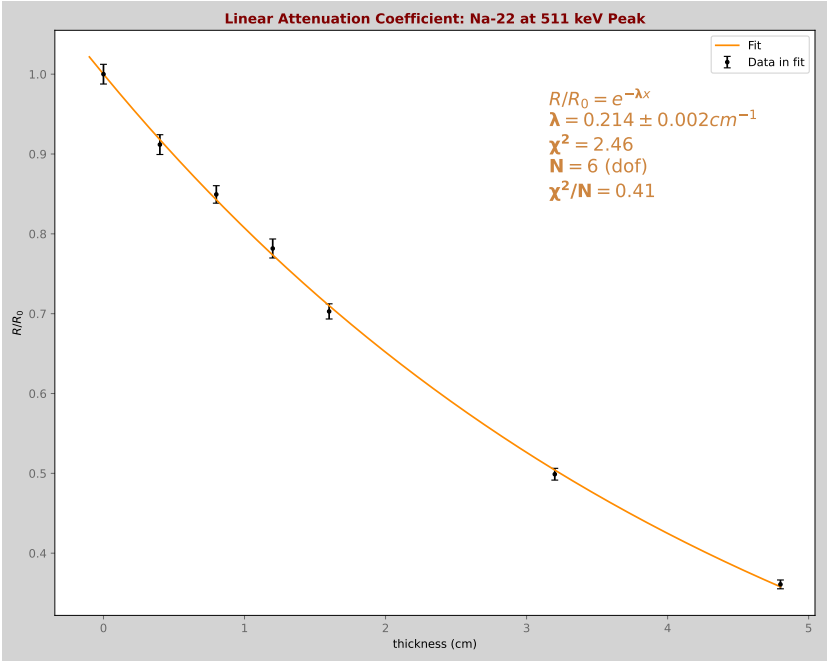

Figure 13: Linear attenuation coefficient fit for Na-22 at 511 keV peak.

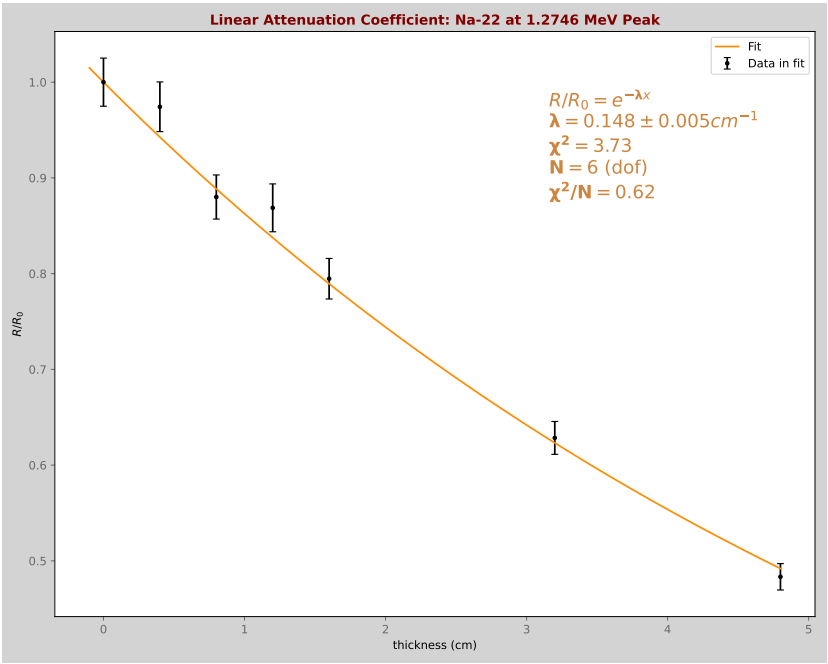

Figure 14: Linear attenuation coefficient fit for Na-22 at 1.2746 MeV peak.

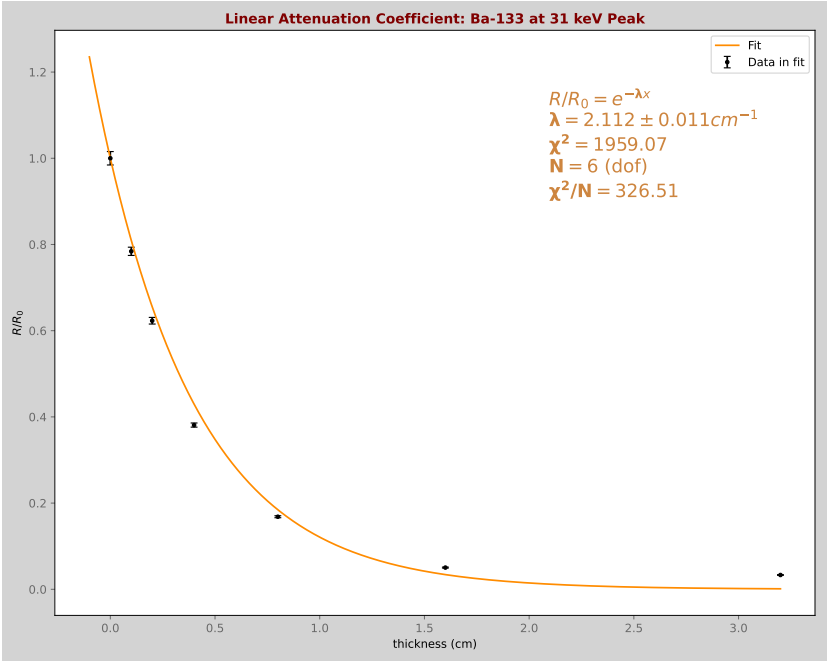

Figure 15: Linear attenuation coefficient fit for Ba-133 at 31 keV peak.

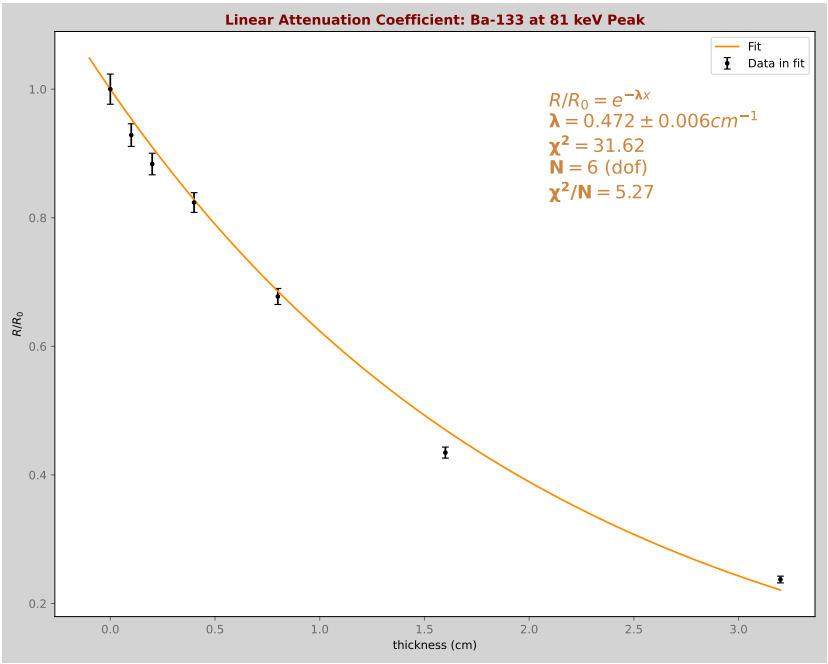

Figure 16: Linear attenuation coefficient fit for Ba-133 at 81 keV peak.

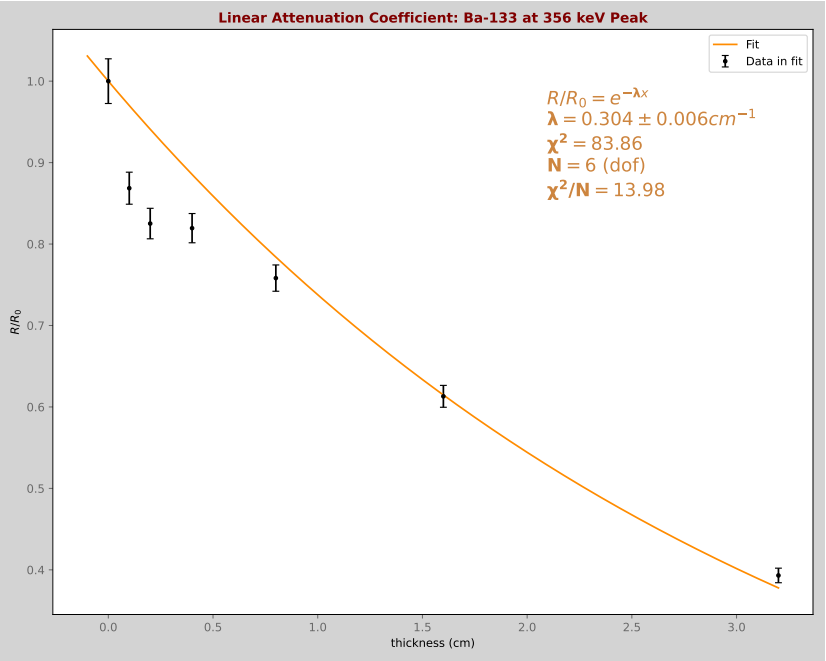

Figure 17: Linear attenuation coefficient fit for Ba-133 at 356 keV peak.

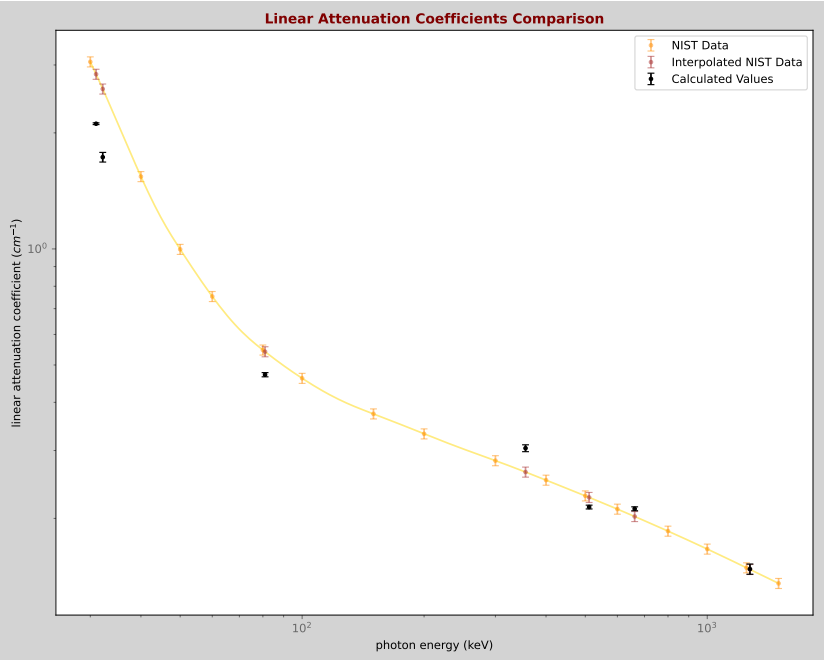

Figure 18: Comparison.

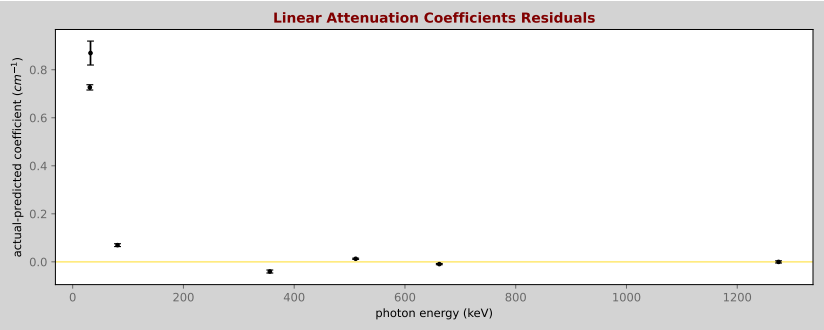

Figure 19: Residuals.